The Zeno Paradox in Quantum Mechanics

Author: Albert Trullols Puigcerver, atrullpu7@alumnes.ub.edu
Facultat de Física, Universitat de Barcelona, Diagonal 645, 08028 Barcelona, Spain.

Advisors: Bruno Julià Díaz, bruno@fqa.ub.edu and Héctor Briongos Merino, hbriongos@fqa.ub.edu

Abstract: The Quantum Zeno Effect (QZE) slows the evolution of a quantum system through frequent measurements, preventing state transitions. In the limit of infinitely fast measurements, the evolution effectively freezes. Quantum Zeno Dynamics (QZD) extends this by confining the system to a subspace of its Hilbert space. This work examines QZD through position and momentum measurements modeled as Von Neumann projections. Frequent measurements confine the system within the projection subspace, leading to remarkable effects near its boundaries. Position measurements induce momentum reversals, while momentum measurements introduce a novel phenomenon of equipotential translocation, opening new research avenues.
Keywords: Zeno dynamics, quantum measurement, quantum evolution, quantum tunneling.
SDGs: Industry, Innovation, and Infrastructure (SDG9).

I. INTRODUCTION

Zeno of Elea, a 5th-century Greek philosopher, was a key figure in the Eleatic School, led by Parmenides, which argued that reality is unchanging and motion is an illusion [1]. His paradoxes, such as the famous "arrow" and "Achilles and the tortoise," contend that motion cannot exist because, at any given moment, an object in motion is at rest in a specific position. These paradoxes, later resolved through calculus and the concept of limits, influenced modern mathematics and physics by introducing ideas of infinite series and continuity. The quantum Zeno effect, named after him, mirrors his paradoxes by describing how frequent observation can freeze the evolution of a quantum system.

Frequent measurements slow the evolution of a quantum system, hindering transitions to states different from the initial one. This phenomenon, known as the quantum Zeno effect (QZE), arises from general features of the Schrödinger equation, leading to quadratic behavior of the survival probability at short times. Von Neumann [2] first identified the connection between short-time evolution and the Zeno effect, though his work on quantum thermodynamics went unnoticed for 35 years. Attention grew with Beskow and Nilsson's [3] suggestion that frequent position measurements in a bubble chamber could prevent particle decay, supported by Khalfin [4] and mathematically formalized by Friedman [5]. The QZE concept was ultimately solidified by Misra and Sudarshan [6], who connected it to Zeno's paradox and blended rigorous mathematics with philosophical reflections. Theoretical until 1988, Cook [7] proposed testing it with oscillating systems, leading to Itano *et al.*'s [8] landmark experiment. Subsequent studies verified the effect in various systems, including photon polarization, nuclear spins, ions, optical pumping, NMR, and Bose-Einstein condensates. In these implementations, the quantum system is confined to its initial state through one-dimensional projections.

Building on the quantum Zeno effect, quantum Zeno dynamics (QZD) [9] extends the concept by showing that frequent measurements can allow a system to evolve within a subspace defined by the measurement process. Unlike QZE, which freezes a system in its initial state, QZD enables evolution within a multidimensional "Zeno subspace" [10]. Grounded in Misra and Sudarshan's theorem [6], this phenomenon broadens the understanding of measurement and quantum evolution. Recently, QZD was observed in a rubidium condensate [11], revealing a superselection rule between two- and three-dimensional subspaces.

In this work, we investigate QZD in the infinite-dimensional Hilbert spaces of position and momentum, with measurements modeled as Von Neumann projections. We first analyze the effects of frequent position measurements on a free particle, observing that, in the limit of many measurements, QZD manifests as unitary evolution confined to the Hilbert subspace defined by the Zeno subspace, subject to rigid Dirichlet boundary conditions [12]. Next, we examine the impact of frequent momentum measurements on a particle interacting with a potential barrier higher than its total energy. This setup leads to momentum reversal classically, as the particle's energy is insufficient to overcome the barrier. As with position measurements, the particle's state in momentum space is confined within the Zeno subspace, resulting in dynamics similar to those observed in position space. We explore both tunneling and non-tunneling particle scenarios.

First, in section II, we establish the foundational framework for the systems under consideration. Next, in section III, we investigate the effects of many position measurements on a free particle. Subsequently, section IV contrasts these findings with the phenomena observed when many momentum measurements are performed on a particle in a potential. Finally, section V concludes the work with a summary of the resulting behaviors.

II. THEORETICAL FRAMEWORK

We consider a particle of mass m initially in the quantum state $|\psi_0\rangle$. The particle is localized around the position x_0 and its motion is constrained to one spatial dimension. It has an initial positive mean momentum p_0, corresponding to a kinetic energy $E_c = p_0^2/2m$. The particle's initial state is always such that it travels from left to right, in the positive x-direction. The incoming particle's wave function has been chosen to be a Gaussian wave packet, which in momentum space is characterized by the central momentum p_0 and the width Δp_0. Following Ref.[13], both space and time have been transformed into dimensionless units. This transformation relies on characteristic lengths of the system. Both x and t are normalized using the width of the incoming wave packet, Δx_0, and the time required for the particle to traverse this packet width Δt_0. According to the Heisenberg uncertainty principle, the wave packet width has been expressed as $\Delta x_0 = \hbar/\Delta p_0$, and the time required for the particle to traverse its own wave function is given by $\Delta t_0 = m\Delta x_0/p_0 = \hbar m/\Delta p_0 p_0$ assuming a speed given by p_0/m. For future mathematical simplicity a factor of 2 has been applied to the temporal normalization factor. The final transformation is given by $\xi = x/(\hbar/\Delta p_0)$ for space and $\tau = t/(2\hbar m/\Delta p_0 p_0)$ for time. The free-particle's speed in these units is $d\xi/d\tau = 2$. The wave-packet representation in the normalized positions space is $\psi(\xi) = (2/\pi)^{1/4} \exp\left[-(\xi - \xi_0)^2\right] \exp(i\kappa_0 \xi)$, with $\kappa_0 = p_0/\Delta p_0$. The time evolution of the wave packet is determined by solving the time-dependent Schrödinger equation (TDSE) using a Crank-Nicolson algorithm (see Appendix 1).

A. The time-dependent Schrödinger equation

In general, our Hamiltonian comprises two contributions: one as kinetic energy from the translational and spreading motion of the wave packet, and another from the interaction with a potential in which the particle is immersed. The specific potentials used will be discussed later. Let $V(\xi)$ denote one such potential, with V_0 as its maximum value. Employing dimensionless units, the TDSE is given by:

$$i\frac{\partial \psi}{\partial \tau} = -\frac{1}{\kappa_0}\frac{\partial^2 \psi}{\partial \xi^2} + \kappa_0 v_0 v(\xi)\psi\,. \tag{1}$$

Parameter κ_0 characterizes the momentum's definition and governs the spreading speed of the wave packet. As κ_0 increases, the conventional momentum-space representation of the wave packet narrows, resulting in a decrease in the spreading speed. We operate in a regime in which $\kappa_0 > 1$, where the wave packet translation dominates over its spreading (see Appendix 2.1). The quantity $v_0 v(\xi)$ rescaled $V(\xi)$ in units of the initial kinetic energy. The parameter $v_0 = V_0/E_c$ relates the particle's kinetic energy to the potential's maximum, while $v(\xi)$ is a normalized potential that retains the shape of $V(\xi)$ but is scaled so that its maximum value is 1.

B. Potential barriers and wells

The study will initially be conducted with a free particle. Later, to induce changes in the particle's momentum, a potential barrier will be introduced into the theoretical setup. A potential barrier, centered at $\xi = 0$, with a height of 1 can be modeled as $v(\xi) = 1/\left[1 + |\xi/\xi_b|^{\alpha}\right]$. Parameter ξ_b represents half the width of the barrier while α is a smoothness parameter. In the limit $\alpha \to \infty$, the potential approaches a square barrier. In this limiting case, the potential is zero everywhere except within the region $[-\xi_b, \xi_b]$, where it equals 1. This potential can be scaled by v_0, defining classically allowed and forbidden regions. According to classical mechanics, if a right-moving particle is placed at $\xi_0 < 0$ such that $\xi_0 < -\xi_b$ (*i.e.*, to the left of the barrier), and if the initial total energy of the particle is purely kinetic, two behaviors are possible. If $v_0 < 1$ (*i.e.*, $E_c > V_0$), the particle is expected to cross the barrier. In contrast, if $v_0 > 1$ (*i.e.*, $V_0 > E_c$), the particle will return at the turning point, where energy conservation is violated. In quantum mechanics, the regime $v_0 > 1$ does not strictly block the particle from crossing the barrier due to quantum tunneling (QT). The wave function undergoes rapid decay within the potential barrier. However, if the wave function extends beyond this decay, there exists a nonzero probability of finding the particle on the opposite side of the barrier. The tunneling probability increases with the spreading speed, and strongly decreases with the barrier's height and width. Thus, under certain conditions involving these three magnitudes, a quantum particle may still be able to cross the barrier (see Appendix 2.2).

A potential well is introduced later in the discussion. It is modeled as $v(\xi) = 1 - 1/\left[1 + |\xi/\xi_b|^{\alpha}\right]$, centered at $\xi = 0$ with height 1. Here, ξ_b represents half the width of the well and α is a smoothness parameter. In the limit $\alpha \to \infty$, the potential approaches a square well. Similarly to the barrier case, when $v_0 < 1$, a classical particle initially placed inside the well and moving to the right is expected to escape. When $v_0 > 1$, the classical particle will turn around as soon as energy conservation is violated, remaining confined inside the well. In a quantum regime, although a fraction of the wave function may extend over the well, no quantum tunneling occurs, as the well's interior is the only classically allowed region.

C. Zeno dynamics via Von Neumann projections

We adopt an operational approach to measurements as selective von Neumann projections, where the measurement of an observable $\hat{A}$ retains only the case within the Zeno subspace defined by the projection, eliminating all wave function components outside the Zeno subspace. This type of measurement is assumed to be performed instantaneously and no re-normalization occurs after each measurement. We perform measurements of normalized position $\xi = x/(\hbar/\Delta p_0)$ and momentum $\kappa = p/\Delta p_0$.

The measurements are computationally represented as the product of a box function, defined by the projection limits, and the wave function in the relevant observable space, either $\psi(\xi)$ in position space or its Fourier transform $\hat{\psi}(\kappa)$ in momentum space. Since we are interested in investigating frequent measurements, the particle's state after N measurements is given by:

$$|\psi_N\rangle = \Pi e^{-iH\Delta\tau} \dots \Pi e^{-iH\Delta\tau} \Pi e^{-iH\Delta\tau} |\psi(0)\rangle \,, \qquad (2)$$

where H represents the Hamiltonian and $\Pi = \int_{a_{\min}}^{a_{\max}} |a\rangle\langle a| \, da$ is the projector onto the Zeno subspace defined by the measurement of $\hat{A}$, which is either $\hat{\xi}$ or $\hat{\kappa}$. The initial state $|\psi(0)\rangle$ is always selected such that it is entirely contained within the Zeno subspace. In this framework, measurements are performed every $\Delta\tau$. At each step between measurements, the wave function's temporal evolution is computed using the Crank-Nicolson algorithm to solve the Schrödinger equation 1.

The survival probability after N measurements (*i.e.*, the probability of the final state being found within the Zeno subspace) is the probability that all measurements lead to an outcome where the intermediate state is found within the Zeno subspace. This probability is given by the product $P_N^S = P_1 P_2 P_3 \dots$, where P_i is the probability of a positive outcome after the i-th measurement. The survival probability P_N^S is expected to approach 1 as $N \to \infty$, in accordance with Misra and Sudarshan's conjecture [6]. Consequently, in this limit, the particle's state is expected to always be found within the Zeno subspace. Since our measurements are defined as Von Neumann projections, the removal of wave function components outside the Zeno subspace leads to a reduction in the norm. As a result, the survival probability after N measurements is given by the square of the norm, $P_N^S = \|\langle\psi_N|\psi_N\rangle\|^2$. In the limit of a large number of measurements, we expect the norm to be preserved, with no further loss of probability.

III. ZENO DYNAMICS VIA FREQUENT POSITION MEASUREMENTS

QZD via position measurements are studied. A Gaussian wave packet, representing a right-moving free particle centered around ξ_0, is employed, with no potential applied. We perform N position measurements defining the Zeno subspace $[\xi_{\min}, \xi_{\max}]$ on the particle's state every $\Delta\tau = \tau_{\max}/N$, with $\tau_{\max}$ denoting the final evolution time. The state after N measurements is given by equation 2, with the Hamiltonian $H = (-1/\kappa_0)\,\partial^2/\partial\xi^2$ and the projector $\Pi = \int_{\xi_{\min}}^{\xi_{\max}} |\xi\rangle\langle\xi| \, d\xi$. The right boundary of the Zeno subspace, $\xi_{\max}$, is chosen such that, in the absence of measurements, the wave packet would extend beyond $\xi_{\max}$, ensuring a nonzero probability of finding the particle for $\xi \geq \xi_{\max}$.

In the absence of measurements, the temporal evolution results in a wave packet centered around $\xi_0 + 2\tau_{\max}$, with increased uncertainty due to its inherent spreading (see Appendix 2.1). This natural progression is illustrated in FIG. 1 (Left), which compares the initial and final profiles of the wave packet. When measurements are introduced, the fraction of the wave packet surpassing the Zeno subspace boundaries is eliminated at each step. As the number of measurements increases, a survival tendency emerges, with fewer components surpassing the Zeno subspace boundary and the removed fraction decreasing. In the limit of many measurements, no components are eliminated, and an interference pattern arises during the interaction, resembling the effect of a virtual wall imposed by the measurements, as shown in FIG. 1 (Right).

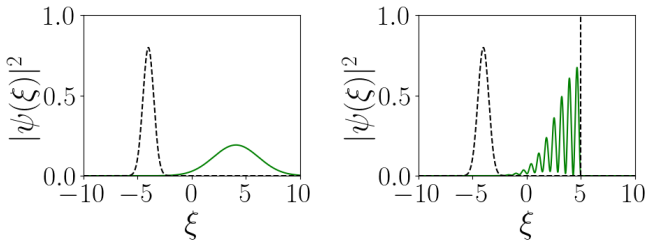

FIG. 1: Free Gaussian wave packet characterized by $\kappa_0 = 4$ and $\xi_0 = -4$ at $\tau_{\max} = 4$ in the absence of measurements (Left) and under $N = 5 \cdot 10^4$ measurements (Right) defined by $\xi_{\max} = 5$. The initial wave packet is shown as a dashed curve. Survival probability is 0.986.

The interaction between the wave packet and the virtual wall formed through measurements results in an effective wave packet reflection and a corresponding momentum reversal. After that, the wave packet freely evolves within the Zeno subspace until it reaches the opposite boundary, where another reflection occurs. The overall dynamics are depicted in FIG. 2, illustrating the wave packet's free evolution within the Zeno subspace, where it remains confined. Upon encountering a boundary, it is reflected by the virtual wall, reversing its expected momentum and continues its evolution in the opposite direction.

This behavior has been repeatedly put forward in the mathematical and physical literature. Zeno dynamics yields ordinary constraints [12]. It is known that if a system has Hamiltonian H and the frequent measurements are checking that the system is within a particular spatial region, then the Zeno dynamics that result are governed by the same Hamiltonian, but with Dirichlet boundary conditions on the boundary of the position subspace defined with the projection. This means that in the limit of $N \to \infty$, the evolution is governed by the Hamiltonian:

$$H_Z = H + v_Z(\xi) \qquad v_Z(\xi) = \begin{cases} 0, & \text{if } \xi \in [\xi_{\min}, \xi_{\max}] \\ \infty, & \text{otherwise} \end{cases} \qquad (3)$$

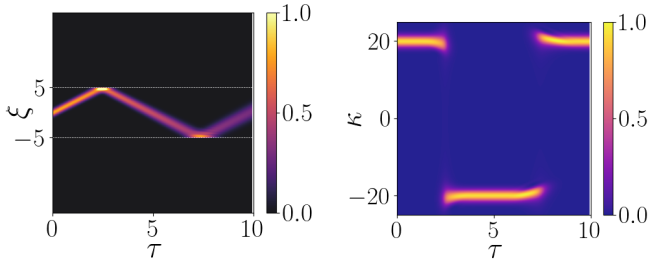

FIG. 2: Temporal evolution of the representation of a free Gaussian wave packet under the regime of frequent position measurements between $\xi_{\min}$ = -5 and $\xi_{\max} = 5$ in position space (Left) and momentum space (Right). The input wave packet is characterized by $\kappa_0 = 20$ and $5 \cdot 10^4$ measurements are performed.

IV. ZENO DYNAMICS VIA FREQUENT MOMENTUM MEASUREMENTS

It has been seen how the interaction between the state and an effective potential v_Z built through measurements induces a momentum reversal, ensuring the state remains confined. This conjugate effect in momentum space due to position measurements motivates the study of the position space consequences of performing momentum measurements. A potential barrier is added to the theoretical setup. Momentum measurements are performed such that the final state is described by equation 2. The Hamiltonian is $H = (-1/\kappa_0)\,\partial^2/\partial\xi^2 + \kappa_0 v_0 v(\xi)$, with $v_0 > 1$ and $v(\xi)$ representing a normalized potential barrier previously introduced in the text. The operator $\Pi = \int_{\kappa_{\min}}^{\kappa_{\max}} |\kappa\rangle\langle\kappa| d\kappa$ represents the projector onto the momentum Zeno subspace $[\kappa_{\min}, \kappa_{\max}]$.

A. Zeno-enhanced quantum tunneling

The result of this operation using a tunneling particle scenario was exposed by Porras *et al.* in Ref.[13] as an attempt to contrast position and momentum measurements, following prior research on QT blocking in a double well by measuring well occupation [14]. The Zeno subspace they used is the positive subset of the κ-space. In this scenario, the tunneling probability equals the survival probability, as in a translation-dominated regime, the fraction of the wave packet with positive momentum directly corresponds to the transmitted fraction. In the limit of many measurements, the momentum direction becomes constrained to remain positive, effectively blocking the fraction of the wave packet that would naturally be reflected by the barrier. This mechanism results in a QT enhancement, which ensures that the entire wave packet tunnels through the barrier. In Ref.[13], it is shown that the number of measurements required to achieve a tunneling probability close to 1 increases as the spreading speed decreases. We contrast the Zeno-enhanced QT in setups with favorable conditions for tunneling and setups where tunneling does not occur, as shown in FIG. 3.

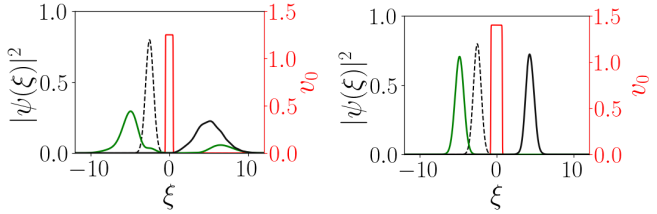

FIG. 3: Tunneling enhancement via QZD for a tunneling particle (Left) and a non-tunneling particle (Right). The dashed curve shows the input wave packet, the green line represents the time-evolved state at $\tau_{\max}$ without measurements, and the black line shows the state at $\tau_{\max}$ with measurements. In (Left), QT probability increases from 0.201 to 0.964 with 400 measurements; setup: $\kappa_0 = 4.5$, $v_0 = 1.25$, $\xi_b = 0.5$, $\tau_{\max} = 4$. In (Right), QT probability rises from 0.000 to 0.976 with 5000 measurements; setup: $\kappa_0 = 30$, $v_0 = 1.4$, $\xi_b = 0.75$, $\tau_{\max} = 3$.

In the absence of measurements, the wave packet representing a tunneling particle (FIG. 3 (Left)) exhibits both reflected and transmitted components. In contrast, for the non-tunneling case (FIG. 3 (Right)), characterized by an increased barrier width and height and a wave packet with a significantly slower spreading speed, the entire wave packet is reflected, resembling classical behavior. When measurements are introduced, both tunneling and non-tunneling wave packets are observed to fully tunnel through the barrier, with the non-tunneling case requiring a higher number of measurements.

B. Zeno-assisted translocation

The observation that a non-tunneling particle can undergo tunneling via QZD when sufficient measurements are performed raises the possibility that what has been described as QT enhancement via QZD for a tunneling particle might, in fact, be better understood as QZD behavior facilitated by QT, rather than the reverse. This interpretation views the enhancement as a reduction in the number of measurements required to reach the QZD many-measurements limit.

We study QZD in non-tunneling setups to isolate its intrinsic effects. By observing the full temporal evolution of a system in this regime, we identify that the interaction with the barrier causes the wave packet to fully transfer between two positions near the barrier boundaries, representing the particle translocation. As shown in FIG. 4 (Left), significant probability density accumulates at these boundary regions during the interaction, while no probability density is detected within the barrier itself. Although tunneling is prohibited in this regime by energy conservation, this principle is upheld, as the particle is never detected within the classically forbidden region where the potential energy exceeds the particle's total energy. If a potential well replaces the barrier and the particle's initial position is set inside the well, a similar phenomenon is observed, with the wave packet transferring between the sides of the well. This behavior is illustrated in FIG. 4 (Top Right).

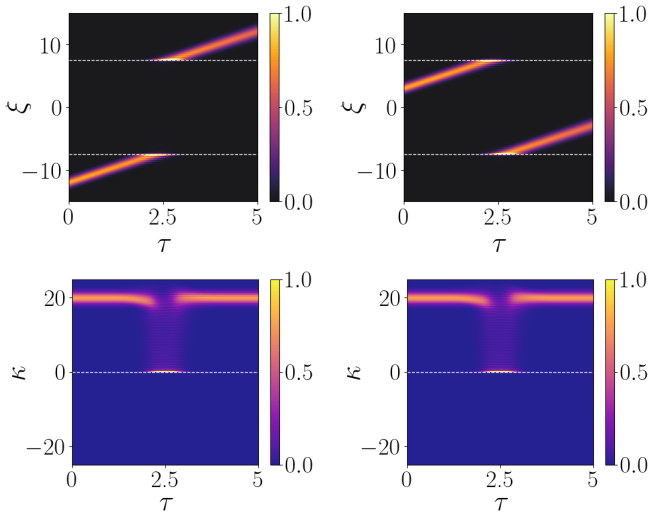

FIG. 4: QZD-assisted translocation in position space (Top) and momentum space (Bottom). In (Left), a potential barrier is used, while in (Right), a potential well is employed. Both potentials have a full width of $2\xi_b = 15$ and height $v_0 = 2$. In (Bottom Left) and (Bottom Right), momentum reversal blocking via QZD with $5{\cdot}10^4$ momentum measurements at $\kappa_{\min} = 0$ is shown for the potential barrier and well, respectively. The survival probability is 0.994 in both cases. The input wave packet is characterized by $\kappa_0 = 20$, $\xi_{0,\text{barrier}} = -12$, and $\xi_{0,\text{well}} = 3$.

From the perspective of momentum space, using a barrier or a well is entirely equivalent. In the absence of measurements, the expected behavior is the one previously depicted in FIG. 2 (Right). The wave packet is completely reflected at one side of the barrier or well, resulting in a reversal of momentum. In FIG. 4 (Bottom Left and Right) we display the cases where many measurements are performed. It is seen how the momentum reversal is suppressed during the interaction with the potential via an effective virtual wall constructed through measurements. This wall is established in momentum space at the boundary of the Zeno subspace between κ_0 and $-\kappa_0$.

At the translocation instants both potential and kinetic energy are conserved individually. The transfer points are defined by the lower boundary momentum of the Zeno subspace $\kappa_{\min}$, which sets a threshold in kinetic energy. Due to total energy conservation, this threshold determines a potential energy value, $v_{\max}$, representing the maximum potential energy achievable by the particle. This value defines the two classical turning points around which the wave packet is transferred. Although this intriguing effect warrants further study, it closely resembles QZD via position measurements where reflections at the boundaries of the Zeno subspace induce a momentum reversal between momentum values of equal kinetic energy. In contrast, the momentum-space representation of the state confinement via QZD results in the wave packet being transferred between positions of equal potential energy.

V. CONCLUSIONS

Quantum Zeno dynamics through frequent measurements, modeled as Von Neumann projections, results in the complete confinement of the state within the Zeno subspace in the limit of many measurements. The boundaries of the Zeno subspace act as rigid walls in the respective observable space. Many position measurements performed over a free Gaussian wave packet leads to a free evolution within the position Zeno subspace with Dirichlet boundary conditions at the boundaries. In momentum space, QZD induces a translocation between equipotential points. Tunneling systems exhibit this behavior at near-unity survival probabilities with significantly fewer measurements compared to non-tunneling systems. The nature, validity regime, and practical applications of Zeno-assisted translocation will be explored in future studies.

Acknowledgments

Thanks to my advisor, Bruno, for his interest, guidance and opportunities. Special thanks to Héctor Briongos for his time, ideas, and contagious passion for physics. Thanks to Roxy for her endless love, and to my parents for their belief and care during this journey.

[1] H. D. P. Lee, *Zeno of Elea*, Cambridge University Press, Amsterdam, 2015.
[2] J. von Neumann, *Die Mathematischen Grundlagen der Quantenmechanik*, Springer, Berlin, 1932.
[3] A. Beskow and J. Nilsson, Arkiv für Fysik 34, 561 (1967).
[4] L. A. Khalfin, Zh. Eksp. Teor. Fiz. Pis. Red. 8, 106 (1968) [JETP Letters 8, 65 (1968)].
[5] C. N. Friedman, Indiana Univ. Math. J. 21, 1001 (1972).
[6] B. Misra and E. C. G. Sudarshan, J. Math. Phys. 18, 756 (1977).
[7] R. J. Cook, Phys. Scr. T 21, 49 (1988).
[8] W. M. Itano, D. J. Heinzen, J. J. Bollinger, and D. J. Wineland, Phys. Rev. A 41, 2295 (1990).
[9] P. Facchi and S. Pascazio, J. Phys. A: Math. Theor. 41, 493001 (2008).
[10] P. Facchi and S. Pascazio, Phys. Rev. Lett. 89, 080401 (2002).
[11] F. Schäfer, I. Herrera, S. Cherukattil, C. Lovecchio, F. S. Cataliotti, F. Caruso, and A. Smerzi, Nat. Commun. 5, 3194 (2014).
[12] P. Facchi, S. Pascazio, A. Scardicchio, and L. S. Schulman, Phys. Rev. A 65, 012108 (2001).
[13] M. A. Porras, N. Mata, and I. Gonzalo, Phys. Rev. A 106, 012220 (2022).
[14] L. Lerner, Eur. J. Phys. 39, 035407 (2018).

La Paradoxa de Zeno a la Mecànica Quàntica

Author: Albert Trullols Puigcerver, atrullpu7@alumnes.ub.edu
Facultat de Física, Universitat de Barcelona, Diagonal 645, 08028 Barcelona, Spain.

Advisors: Bruno Julià Díaz, bruno@fqa.ub.edu and Héctor Briongos Merino, hbriongos@fqa.ub.edu

Resum: L'efecte Zeno quàntic o QZE (Quantum Zeno Effect) retarda l'evolució d'un sistema quàntic mitjançant mesures freqüents, evitant les transicions d'estat. En el límit de mesures freqüents, l'evolució queda efectivament congelada. La dinàmica Zeno quàntica o QZD (Quantum Zeno Dynamics) amplia aquest concepte confinant el sistema a un subespai del seu espai de Hilbert. Aquest treball examina la QZD mitjançant mesures de posició i moment modelades com projeccions de Von Neumann. Les mesures freqüents confinen el sistema dins del subespai de projecció, donant lloc a efectes notables prop de les seves fronteres. Les mesures de posició indueixen reversions de moment, mentre que les mesures de moment introdueixen un fenomen nou de translocació equipotencial, obrint noves vies d'investigació.

Paraules clau: Dinàmica Zeno, mesura quàntica, evolució temporal quàntica, efecte túnel.

ODSs: Aquest TFG s'alinea amb l'ODS9 (Indústria, Innovació i Infraestructures) ja que explora dinàmiques quàntiques que podrien contribuir al desenvolupament de tecnologies innovadores i infraestructures en àrees com la computació quàntica i la informació quàntica.

APPENDIX 1: TDSE NUMERICAL SOLUTION VIA CRANK-NICOLSON ALGORITHM

The temporal evolution of the wavefunction is obtained by numerically solving the time-dependent Schrödinger equation (TDSE) using the Crank-Nicolson method. This method, being unitary, ensures the preservation of the wavefunction's norm throughout its evolution. To derive the numerical representation of our TDSE, we utilize the following discretizations:

$$\begin{aligned} \frac{\partial \psi}{\partial \tau} &\rightarrow \frac{\psi^{j+1} - \psi^{j}}{\Delta \tau}, \\ \frac{\partial^2 \psi}{\partial \xi^2} &\rightarrow \frac{1}{2}\left(\frac{\psi_{n+1}^{j+1} - 2\psi_{n}^{j+1} + \psi_{n-1}^{j+1}}{(\Delta \xi)^2} + \frac{\psi_{n+1}^{j} - 2\psi_{n}^{j} + \psi_{n-1}^{j}}{(\Delta \xi)^2} \right), \\ \psi &\rightarrow \frac{\psi^{n+1} + \psi^{n}}{2}. \end{aligned} \tag{4}$$

The upper and lower indices have been defined as temporal and spatial indices, respectively, such that $\psi^n = \psi(\xi, \tau_n)$, $\psi^{n+1} = \psi(\xi, \tau_n + \Delta\tau)$ and $\psi_j = \psi(\xi_j, \tau)$, $\psi_{j\pm1} = \psi(\xi_j \pm \Delta\xi, \tau)$. By substituting discretizations 4 into equation 1 and following the necessary algebraic steps, we obtain the implicit matrix equation (5).

$$\hat{A}\psi^{j+1} = \hat{B}\psi^{j} \tag{5}$$

With trigonal matrices $\hat{A}$ and $\hat{B}$ defined as:

$$\hat{A} = \begin{pmatrix} 1+\alpha+\beta v(\xi) & -\alpha/2 & 0 & 0 & \cdots \\ -\alpha/2 & 1+\alpha+\beta v(\xi) & -\alpha/2 & 0 & \cdots \\ 0 & -\alpha/2 & 1+\alpha+\beta v(\xi) & -\alpha/2 & \cdots \\ 0 & 0 & -\alpha/2 & 1+\alpha+\beta v(\xi) & \cdots \\ \vdots & \vdots & \vdots & \vdots & \ddots \end{pmatrix} \quad \alpha = \frac{i\Delta\tau}{\kappa_0 (\Delta\xi)^2}$$

$$\hat{B} = \begin{pmatrix} 1-\alpha-\beta v(\xi) & \alpha/2 & 0 & 0 & \cdots \\ \alpha/2 & 1-\alpha-\beta v(\xi) & \alpha/2 & 0 & \cdots \\ 0 & \alpha/2 & 1-\alpha-\beta v(\xi) & \alpha/2 & \cdots \\ 0 & 0 & \alpha/2 & 1-\alpha-\beta v(\xi) & \cdots \\ \vdots & \vdots & \vdots & \vdots & \ddots \end{pmatrix} \quad \beta = \frac{i\Delta\tau\kappa_0}{2}$$

To ensure both numerical precision and stability, we have selected small values for the spatial and temporal steps, $\Delta\xi$ and $\Delta\tau$, respectively, satisfying to the condition $C < 0.4$ with $C = (1/\kappa_0)\Delta\tau/\Delta\xi^2 + \kappa_0 v_0 \Delta\tau$. In FIG. 5, it is shown that decreasing the temporal step $\Delta\tau$ (and thus C) for a fixed spatial step $\Delta\xi$ improves numerical precision. FIG. 5 (Left) compares wave packet dispersion evolution in time, while FIG. 5 (Right) shows the total energy normalized to the survival probability for various $\Delta\tau$ values, highlighting agreement with the expected constant energy.

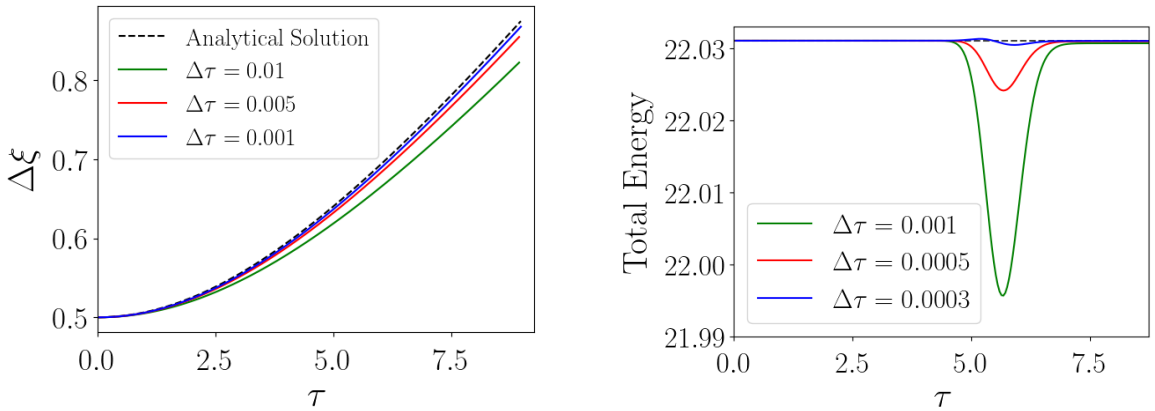

FIG. 5: Temporal evolution of a Gaussian wave packet dispersion (Left) and of the total energy of the system for different values of the temporal step $\Delta\tau$. Energy conservation is studied in a setup containing a narrow barrier where the evolution becomes challenging to compute.

APPENDIX 2: GAUSSIAN WAVE PACKET DYNAMICS

Assume the preliminary foundations exposed in Section II representing a 1D right-moving particle of mass m initially located around x_0 with a momentum p_0 with uncertainty Δp_0. Let $\xi = x\,(\hbar/\Delta p_0)$ and $\tau = t/\,(2\hbar m/\Delta p_0 p_0)$ be the normalized position and time coordinate, respectively. The wave function representation in the normalized position space takes the form of the Gaussian wave packet $\psi(\xi) = (2/\pi)^{1/4} \exp\left[-(\xi - \xi_0)^2\right] \exp(i\kappa_0 \xi)$, with $\xi_0 = x_0/\,(\hbar/\Delta p_0)$ and $\kappa_0 = p_0/\Delta p_0$.

APPENDIX 2.1: Free Gaussian Wave Packet Dynamics

The free evolution of a Gaussian wave packet is characterized by two distinct types of displacement: translation, corresponding to the propagation of the wave packet, and spreading, arising from the superposition of waves with different momenta and velocities. Translation can be analyzed by tracking the time evolution of the wave packet's central position, while spreading is studied through the time evolution of the square root of the positional variance of the wave function. The time evolution of a Gaussian wave packet can be determined analytically.

For a Gaussian packet representing a particle of mass m, the center is expected to undergo uniform rectilinear motion in conventional position space with a velocity p_0/m. Considering the rescaling employed in this study, the time evolution of the center of the Gaussian packet, initially centered at ξ_0, is given analytically by:

$$\langle \xi \rangle\,(\tau) = \xi_0 + 2\tau \tag{6}$$

On the other hand, the wave packet spreading over time is inherently tied to the choice of variables, as the normalized momentum $\kappa_0 = p_0/\Delta p_0$ corresponds directly to the width of the Gaussian wave packet in non-normalized momentum space. The spreading of the Gaussian wave packet is given by:

$$\Delta\xi(\tau) = \Delta\xi(0)\sqrt{1 + \left(\frac{\tau}{\Delta\xi(0)^2\kappa_0}\right)^2} \quad \text{where} \quad \Delta\xi(0) = \sqrt{\langle\psi(0)|\xi^2|\psi(0)\rangle - \left(\langle\psi(0)|\xi|\psi(0)\rangle\right)^2}\,, \tag{7}$$

with $\langle\psi(0)|\xi|\psi(0)\rangle$ simply being ξ_0. It is straightforward to demonstrate that $\langle\psi(0)|\xi^2|\psi(0)\rangle = 1/4 + \xi_0^2$, leading to $\Delta\xi(0) = 1/2$.

In FIG. 6, the evolution of the wave packet's central position and its dispersion over time, as obtained from a simulation using our Crank-Nicolson algorithm, are plotted and compared with the expected analytical results given by equations 6 and 7, respectively. The agreement between the numerical and analytical results is clearly observed.

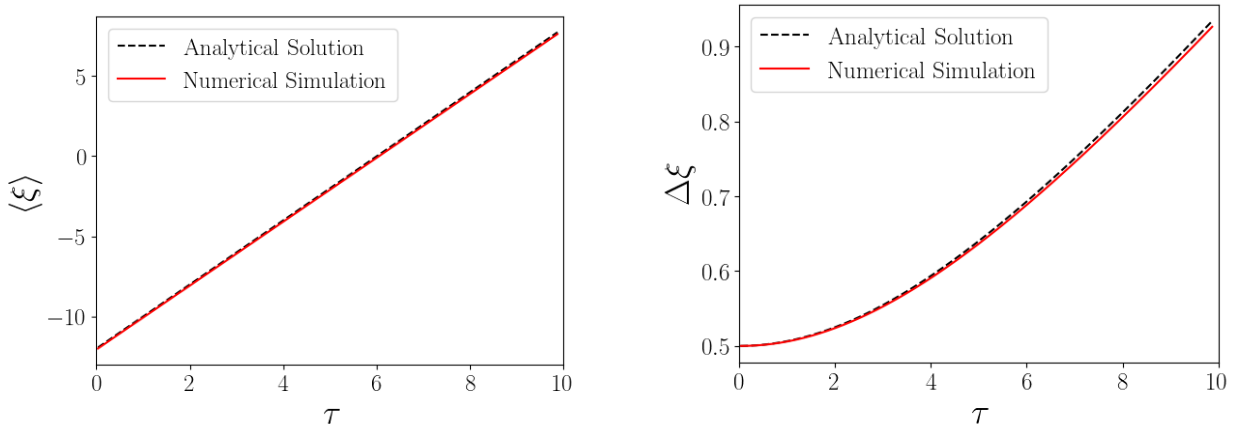

FIG. 6: Temporal evolution of a Gaussian wave packet's central position (Left) and dispersion (Right) plots. The central position is calculated as the expected value of the normalized position operator, while the dispersion is calculated as the standard deviation of the normalized position operator. The exact result is represented by a black dashed line, and the results from a numerical simulation are represented by a red solid line. The wave packet is characterized by $\kappa_0 = 25$.

Both displacement modes contribute to the total kinetic energy of the system. The relative dominance of these contributions defines distinct dynamical regimes, which can be analyzed as a function of the parameter κ_0. For $\kappa_0 < 1$ ($p_0 < \Delta p_0$), the dominant contribution to the kinetic energy arises from spreading, causing the wave packet to spread faster than it translates. Conversely, for $\kappa_0 > 1$ ($p_0 > \Delta p_0$), translation dominates, resulting in slower spreading. In the case $\kappa_0 = 1$ ($p_0 = \Delta p_0$), translation and spreading contribute equally to the total energy. In FIG. 7 (Left), as κ_0 increases, the wave packet becomes less spread out after time τ. For the minimum κ_0, spreading dominates over translation, causing rapid deformation of the wave packet. For the maximum κ_0, the behavior approximates the classical limit, where spreading is negligible and translation dominates. In FIG. 7 (Right), this is illustrated by the energy contributions from spreading, where $\langle T_{\text{trans}} \rangle = \kappa_0$. The spreading-dominated and translation-dominated regimes are identified based on whether the energy contribution from spreading is higher or lower than that from translation, *i.e.*, κ_0. Notably, when $\kappa_0 = 1$, both contributions are equivalent.

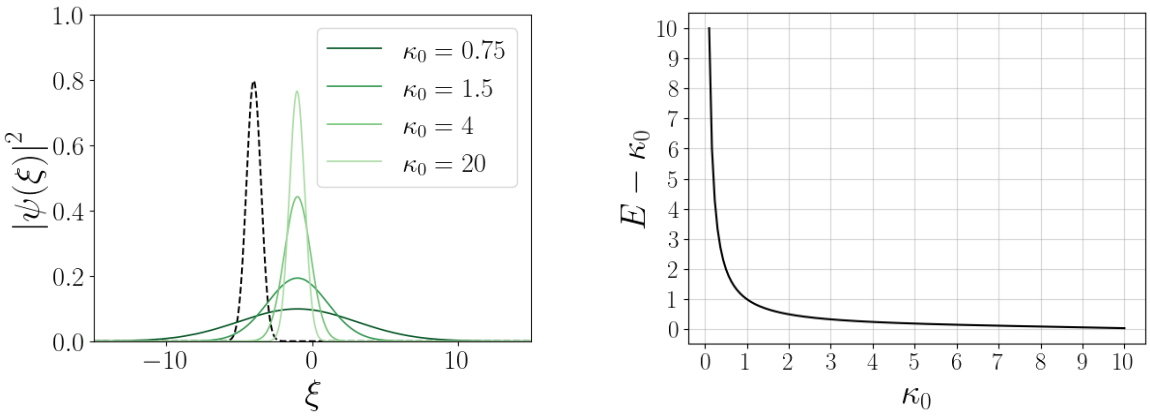

FIG. 7: (Left) Comparison between the input wave packet (dashed line) and the wave packet at time $\tau = 1.5$ (solid red line) for different values of normalized initial momentum κ_0. (Right) Evolution of the energy contribution from the spreading of a free wave packet as a function of the normalized central momentum κ_0.

APPENDIX 2.2: Gaussian Wave Packet Tunneling Dynamics

Quantum tunneling is the phenomenon where particles traverse regions with potential energy exceeding their total energy, enabled by intrinsic uncertainties in position and momentum. The wavefunction extends into classically forbidden regions, where the probability density decays exponentially. The system's transmittance depends on the barrier's height and width. In FIG. 8, the transmittance through a potential barrier, *i.e.*, the tunneling probability, is represented as a function of the barrier's width and height. In both cases, significantly fast decays are observed.

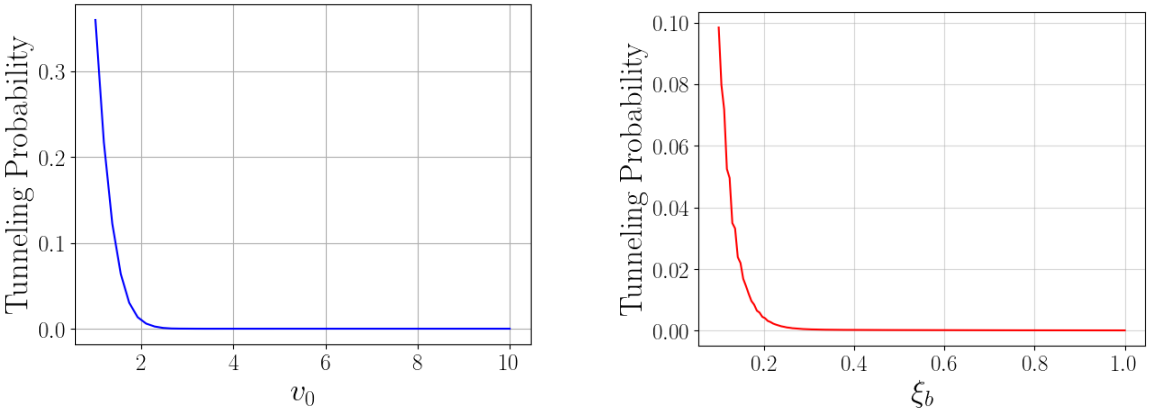

FIG. 8: Decays associated with the entry of a Gaussian wave packet with $\kappa_0 = 5$ into a potential barrier as a function of the half-width ξ_b (Left) and the relative height of the barrier v_0 (Right). The evolution is carried out up to $\tau = 6.2$. In the study of the width dependence, the relative barrier height is fixed at $v_0 = 4$ and the width is fixed at $\xi_b = 1$ in the study of the relative height. In both cases, the smoothness is set to $\alpha = 100$

Given that the wave function under consideration is represented in the normalized position space as a Gaussian wave packet, it is intuitive to recognize that the wave packet's spreading significantly influences the tunneling probability. We simulate a setup involving a particle approaching a potential barrier described by $v_0 v(\xi)$, where $v_0 = V_0/E$, with V_0 representing the maximum potential energy of the barrier and E denoting the total energy of the particle. The function $v(\xi)$ is characterized by a full width at half maximum of $2\xi_b$. Our regime of interest satisfies $v_0 > 1$, ensuring that the particle is classically forbidden from crossing the barrier to maintain energy conservation.

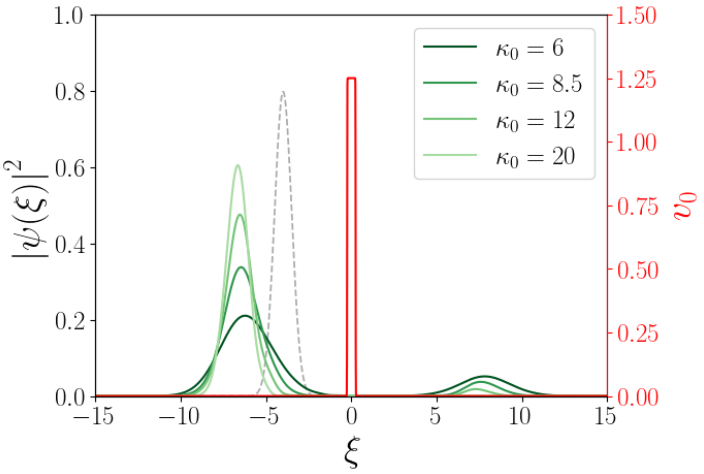

FIG. 9: Quantum tunneling dependence on κ_0. The barrier width and height are held constant. For increasing values of κ_0, the tunneling probabilities are 0.194, 0.093, 0.035, and 0.000, respectively. The wave packet evolves until $\tau = 5$, using a barrier width of $\xi_b = 0.25$ and a barrier height of $v_0 = 1.25$.

In FIG. 9, it becomes visible how fast-spreading wave packets (low κ_0) exhibit better tunneling probability than those that spread slower. This probability decreases with κ_0, and when κ_0 is high enough, the tunneling fraction of the wave packet becomes negligible, with the wave packet being almost completely reflected by the barrier, resembling a classical limit.